Changes in surface velocities over four decades on the Laurichard rock glacier (French Alps)

Emmanuel Thibert, Xavier Bodin

Received: 28 July 2021 | Revised: 1 June 2022 | Accepted: 7 June 2022

DOI: 10.1002/ppp.2159

RESEARCH ARTICLE

WILEY

Changes in surface velocities over four decades on the Laurichard rock glacier (French Alps)

Emmanuel Thibert[1] | Xavier Bodin[2]

[1]Université Grenoble Alpes, INRAE, UR ETGR, Saint-Martin-d'Hères, France

[2]Université Savoie Mont-Blanc, CNRS, EDYTEM, Chambéry, France

Correspondence
Emmanuel Thibert, Université Grenoble Alpes, Irstea, UR ETGR, 2 rue de la Papeterie-BP 76, F-38402 Saint-Martin-d'Hères, France.
Email: emmanuel.thibert@inrae.fr

Funding information
All'Envi; CryobsClim; Parc National des Ecrins; PermaFrance; OSUG

Abstract

The longest time series of surface velocities recorded on a rock glacier in the French Alps, covering more than three decades, has been recorded since 1983 on the Laurichard rock glacier (Ecrins range). The time signal of velocity changes is extracted from variance analyses separating time and space variabilities on the rock glacier surface to provide an average-wide time signal. We show that changes in velocity from year to year are virtually uniform at all locations with homogeneous accelerations or decelerations on the scale of the rock glacier as a whole. The spatial structure of velocity was found to be nearly at steady state over 35 years. Nonlinear effects are located in low-velocity areas such as the rock glacier margins where accelerations/decelerations tend to be proportional to the local velocity. Over the period of record, a long-term trend in rock glacier acceleration was detected with a rate of +0.2 m/yr per decade. Two main phases of acceleration were identified from the mid-1980s to 1999 and from 2010 to 2015. In between, those two periods were interrupted by a 10-year period of almost steady-state velocities with an abrupt deceleration from 2006 to 2009 of −0.35 m/yr. The process of internal increases in ice temperatures alone (and associated changes in creep rates) would seem insufficient to explain the long-term rise of surface velocities and their annual variations. Changes in the liquid water are a possible contributing factor, due to the injection of seasonal water caused by melting snow cover or internal melt due to heat generated by enhanced ice creep and friction in the ice/debris mixture.

KEYWORDS
rock glacier acceleration, rock glacier kinematics, spatial and temporal variability, surface velocity

1 | INTRODUCTION

Rock glaciers are creeping mixtures of ice and debris that exist mainly in areas of discontinuous permafrost in relatively dry mountains.[1] The thermal inertia of permafrost and the mechanical properties of rock glaciers lead them to react to long-term climatic trends,[2] but also to short-term fluctuations when water is involved in the dynamics.[3,4] Since the 1980–90s, time series of Alpine rock glacier surface velocities have reported synchronous accelerations[5–9] and even structural disintegration or destabilization.[6,10–13]

Changes in creep velocities have been empirically linked to climate drivers/derivatives such as air or ground temperature,[14–19] snow

cover/melt, and liquid precipitation (e.g.,[14,20,21]). Cooling and slowing down during the early winter months under slight snow-cover conditions has also been noted.[22]

Nevertheless, inferring climate drivers involved in surface-velocity changes is not an easy task. Year-to-year changes in velocities are not always easily explained. Direct correlations with weather variables are poor,[23,24] possibly due to time lags between triggers and responses,[25] and statistical links may be essentially driven by the inherent long-term trends of the time series.

Linking surface kinematics of rock glaciers to climate drivers requires maintaining an *in situ* network of markers and their geodetic survey over decades or operating with remote sensing techniques (e.g.,[26–31]). The necessary long series on velocity are scarce. The oldest time series worldwide has been recorded at the Äußere Hochebenkar rock glacier in Austria since 1938.[23,24,32] For the European Alps, only five series of annual surface-velocity *in situ* measurements extend over more than 20 years. They represent a small sample (14%) among the 34 rock glaciers monitored for surface velocity.[9] Long series are often affected by missing values, which can be missing point-measurements in some years or missing years (i.e., at every location). Under such conditions, retrieving an annual average velocity time signal free from measurement biases is difficult. An interesting option is the analysis of variance (ANOVA) that separates the overall annual variation from the spatial variability of velocity on the surface of rock glaciers (e.g.,[33,34]). With this approach, missing values can be reconstructed using information from other measurements on the rock glacier surface without any external assumptions, simply from the correlation structure of the data.

In the French Alps, the longest monitoring activities (since 1979) on a rock glacier concern the Laurichard glacier.[35] They are the second longest in Europe, after Äußere Hochebenkar in Austria.[23,24,32] Here, we propose to analyze this long time series of surface velocities using ANOVA. The goal is to retrieve a rock glacier-wide velocity time signal which accounts for missing values. Section 2 presents details of the site and of the main previous studies. Velocity data and their treatment via ANOVA are presented in Section 3. The reconstructed time signal of velocity changes is presented in Section 4. Section 5 discusses the results of variance analysis and analyzes internal processes that might drive velocity changes.

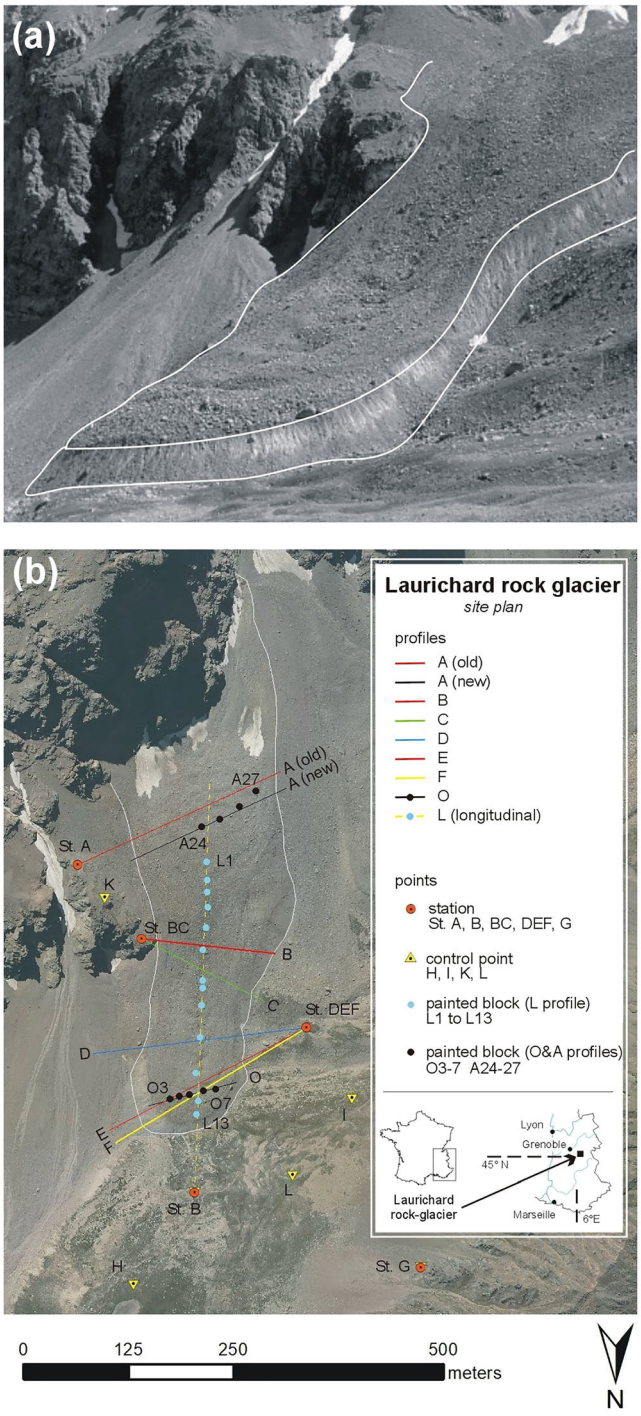

FIGURE 1 (a) Laurichard rock glacier on the north slope of Combeynot, Combe de Laurichard, Ecrins range, southern French Alps (45.01°N, 6.37°E). (b) Location of surface-velocity measurement points (average location of painted rocks over 28 years) along the longitudinal profile of Laurichard rock glacier, the topographic station, and control points [Colour figure can be viewed at wileyonlinelibrary.com]

2 | STUDY SITE

The Combe de Laurichard is a well-investigated watershed largely covered with discontinuous (50–90% of the landscape) mountain permafrost, located in the southern French Alps (45.01°N, 6.37°E; Figure 1). The main active rock glacier, initially named RGL1,[35] extends from 2,650 m a.s.l. at the rooting zone to 2,450 m a.s.l. at the toe. It is 490 m long, between 80 and 200 m wide, and has an apparent thickness of 15–25 m based on ground-penetrating radar investigations.[36] The apparent thickness is consistent with the heights of the lateral and frontal margins. It displays morphological features typical of an active landform such as the presence of transverse ridges and furrows, as well as steep and unstable lateral and frontal talus.

According to field observations and geophysical data,[36,37] the internal structure can be divided into three main sections:

- the upper third in which a high proportion of ice, with massive bulk ice that has been detected (apparent resistivity value >2 × 10^6 Ω.m) and observed (within a temporary vertical section, similar to a rimaye, formed in summer 2003), and a probable thickness of the rock glacier of 20–25 m, including an active layer thickness of 1–3 m;
- the median third, in the steepest part of the rock glacier, is visually thinner (around 15 m) and probably contains a lower proportion of ice. The upslope of the massive ice body is stretched by the creeping mass and the ice is probably more heterogeneous in terms of proportion, structure, and thermo-hydric state;
- the tongue (lower third) of the rock glacier has a probable thickness of 20–25 m, a low proportion of ice, and a heterogeneous spatial distribution. The low resistivity values suggest temperate ground ice with possible liquid water.

Due to its location in the internal Alps, this area experiences rather dry and cold climatic conditions on a north-facing mountainside in a transitional climate zone between the northern French Alps, characterized by a weak oceanic regime, and the southern French Alps, generally subject to Mediterranean influences. From SAFRAN weather data re-analyses,[38] the mean zero-isotherm altitude (ZIA) in the Laurichard area is estimated to be around 2,450 m a.s.l. (1981–2010 reference period), i.e., the elevation of the bottom of the rock glacier. Mean annual precipitation is ∼1,150 mm at this elevation and the mean duration of snow cover is ∼220 days per year.[26,39]

The rooting zone of the rock glacier is supplied by debris originating from a highly fractured 600-m-high, granitic rock face. This gravitational activity feeds the rock glacier with relatively large boulders (typically 0.1–1 m in size) at high debris-production rates (0.2–0.3 m/century[40]). The couloirs that cut the rock face also channel snow avalanches and contribute to accumulating 1–2-m-thick long-lasting snow patches at the foot of the rock face. As a result, a multilayer structure is often found there, with layers of debris alternating with snow and refrozen ice from melting snow.

3 | MATERIALS AND METHODS

3.1 | Block positions and velocities

Surface velocities have been monitored since 1983 and are derived from annual displacements of painted blocks.[35] In this study, we used the initial and oldest longitudinal (L) profile of 13 blocks set up in 1983, which provides the longest time series of velocities (L1–L13; Figure 1[26,37]). Block positions were first measured with theodolites (e.g., Kern DKM1; Wild T1 with additional laser distance meter) from reference stations previously surveyed on control baselines. From the 1990s to 2013, total stations (Sokkia set 3C, Leica TS02) were then used from the main reference station at the bottom of the longitudinal profile (Figure 1). Coordinates were measured in a local system using control (orientation) points. Since 2012, positioning has been achieved using a geodetic differential GNSS (L1 & L2 frequencies; GPS and GLONASS constellations, LeicaGeosystems GS10 receiver) with a reference receiver set at the main station (reference-to-rover baseline between 50 and 420 m). A transversal profile (O) was set up in 2008 (Figure 1). Velocities along this profile are used here for validation in the variance analysis of section 4.4. Former transverse profiles (A–F) initiated in 1979 and 1983[35] are also displayed in Figure 1.

Errors in theodolite and GNSS measurements were calculated each year from control points located on nonmoving blocks outside the rock glacier. The margin of error in annual displacements is ±0.04–0.06 m, which is acceptable considering observed annual displacements on the rock glacier surface from 0.2 to 2 m. To avoid biases and ensure continuity in the data series, rock displacements were monitored by the two techniques (theodolite versus GNSS) in 2012 and 2013. The consistency is acceptable with discrepancies of ±0.09 m between the two surveys (Appendix). The former local coordinate reference system was changed to a global one with the GPS survey and we chose the Lambert conic conformal projection (zone III) to minimize distortion in distance to less than 7 cm/km in the transformation of the coordinates. Regarding error estimations, velocity is a displacement per year which results from the difference in two position measurements, and its error is thus given by the quadratic sum of the annual error in positioning (maximum of 0.06 m). This equals $(0.06)^2 + (0.06)^2$ which gives 0.085, rounded up to 0.1 m/yr, assuming uncorrelated errors from year to year.[41]

From 1983 to 2000, displacements were measured along the local *y*-axis only (close to the steepest slope line; the white dashed line in Figure 1b), which is the direction of the longitudinal profile shown in Figure 1. The perpendicular component to the main flow line was not recorded. As determined from the 2000s and later measurements along both axes, this does not affect velocity estimations because 96% of the displacement is along the longitudinal profile. Moreover, for the year-to-year velocity changes analyzed in the present study, this lack of the *x*-axis component has a negligible effect given that changes are captured by the two components identically. Elevations were also measured so that horizontal displacement changes could be discriminated from vertical changes due to the slope. To calculate annual velocities from displacements, we accounted for variable survey dates from year to year. Annual velocities were then first calculated from displacements between survey dates and later rescaled to annual steps. Leap years have been taken into account. The same rocks have been used on this longitudinal profile throughout the record. No rock renewal was undertaken and this Lagrangian frame of observation must be taken into account in analyzing the spatial structure of the velocity in the Eulerian frame (see section 3.2). Note that block positions are associated with a date of measurement, while velocities refer to a period of displacement within a year or a multiple year time period. Using the average of two subsequent measurement years, we chose the integer portion of this average to conventionally identify the period for velocity (see "missing years" below). The complete data set of horizontal velocity values for each of the painted rocks is provided in Table A1 of the Appendices.

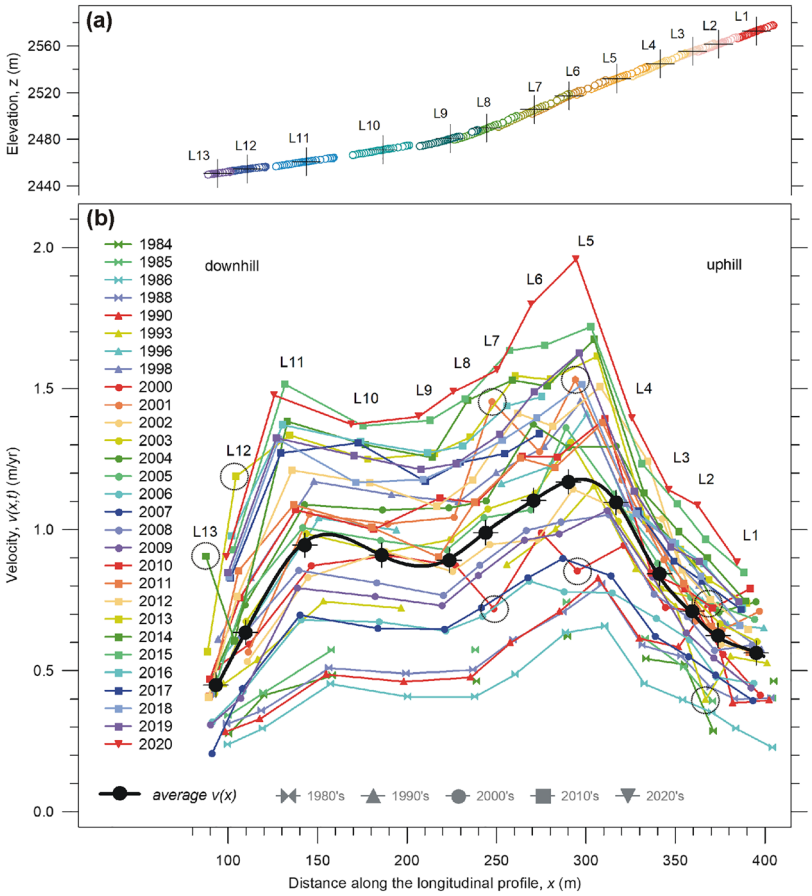

FIGURE 2 (a) Elevations of painted rocks along the longitudinal profile over the four decades of the record (raw data). Black crosses plot the average positions of each rock and the round markers their annual positions along the flow. (b) Annual velocities of block versus positions along the longitudinal profile as recorded from 1984 to 2020. The average velocity profile is the mean velocity of each block plotted as a function of the average block position over the record (black markers). The black curve is the interpolated profile of velocity, $v(x)$, used to correct the velocity due block displacements. The same markers are used per decade (in gray at the bottom), and same colors are used for unit numeration of years within decades. Circles denote data for which measurement errors in position are suspected due to large discrepancies in the overall variance (outliers due to block sliding, tilting or gross measurement error) [Colour figure can be viewed at wileyonlinelibrary.com]

Over the three decades of the record, some velocity data are inevitably missing in the series and two types of deficiency must be taken into account.

- *Missing years*. The temporal survey is almost continuous on an annual basis. The survey was effectively carried out in the first three years (1984, 1985, 1986) and then continuously from 2000 to 2020. In between, some years are missing and only average velocities are available from cumulative displacements over a multiple year time period. This occurred over three periods of three years (1986–89, 1991–94, and 1994–97) and two periods of two years (1989–91 and 1997–99).
- *Missing positions*. In some years, some blocks were not measured because they were untraceable (paint marking disappeared, not found, etc.). In 2015, block L13 reached the rock glacier snout, then tilted and fell down the frontal talus.

Horizontal velocities along the longitudinal profile are displayed in Figure 2b for the 29 years of observations between 1983 and 2020.

3.2 | Correction of flow displacement

The same rocks have been used throughout the record on the longitudinal profile, and a Lagrangian-type observation has been adopted (the observer follows each individual block as it moves through space and time). Therefore, displacements from year to year change block locations in the spatial structure of the velocity. Consequently, velocity changes at a block result also to some extent from rock displacement along the flow line and its position over time. This effect is not a time effect driven by external controlling factors (meteorological conditions, long-term climate drivers), but a spatial effect that must be corrected to extract the proper time signal in velocity changes at a fixed location. This correction converts in a Eulerian analysis framework (a way of looking at motion that focusses on specific locations in space as time passes).

Cumulative displacements and elevation changes are displayed in Figure 2a. Figure A2 (Appendix) specifically plots horizontal and elevation changes as a function of each year of the record. On average, displacements amounted to 30 m in 2020, with elevation losses of up to 15 m. The average distance between blocks is 28 m, and therefore in 2020 some blocks had reached the position that the block just below had at the beginning of the survey (the upper rocks L1, L9, L12). Some even exceeded this position (L2–L8). Only the lowest rock flow lines (L10, L11, and L13) remained disconnected (Figure 2a). Clearly, for the subsequent analyses, block position and its effect on velocity had to be accounted for. To correct velocity changes along the flow line of the longitudinal profile, we used the average block positions and fitted each position using a cubic spline function (Figure 2b). This velocity function was used for each year of the record to calculate velocity

changes due to displacement of the block along the profile. To illustrate the range of this effect, corrections were calculated using the velocity at the average position of the 1984–2020 survey (Figure 3). In regions where the velocity decreased along the flow (L6–L9, L11–L13), differences are positive before the blocks reach their average position and negative once the blocks exceed the average. In regions where block velocity increased along the flow (L1–L5), deviations are negative before and positive after. Block L6 encounters both conditions. These differences have been used as corrections. They were subtracted from the annual velocity values according to the block positions along the profile (Figure A2 in the Appendix). They are non-negligible and can reach more than 20% of the average velocity of blocks (Figure 3). For example, block L12 decelerates during 2010s and 2020s due to a lower slope downstream and deviations from its average velocity reach −0.13 m/yr. During the 1980s and 1990s, the block was in a steeper slope area of the profile and the deviation from the average velocity reaches +0.14 m/yr.

3.3 | Variance analysis

In this section, we analyze the spatial distribution of the velocities at the rock glacier surface and the way velocities change from year to year. This analysis is free from any hypothesis on the mechanical properties of the creeping material within the rock glacier body, its rheology, or its constitutive relationship (strain rate to shear stress relationship). This approach considers only the rock glacier kinematics (surface velocity data) and their spatio-temporal variability.

Two remarkable features stand out in Figure 2b. The first is that annual velocity profiles are shifted (translated) from year to year by an amount that is roughly the same for all blocks. This is made graphically clear by the velocity profiles running virtually parallel above or below the average velocity profile, which is plotted by the black line. If $v(x,t)$ denotes the velocity for year t at position x on the longitudinal profile and $\boldsymbol{v}(x)$ is the average velocity at the same position over the whole period of record, this feature can be written as follows:

$$v(x,t) = \boldsymbol{v}(x) + \Delta\beta(t). \quad (1)$$

Equation (1) states that velocity deviations from the average $v(x,t)$-$\boldsymbol{v}(x)$ are the same at any point of the profile and just a function of time $\Delta\beta(t)$, which represents the time signal in velocity changes. This time signal is the same at all measurement points. It is homogeneous at the rock glacier surface and is therefore a rock glacier-wide signal. It represents the overall linear acceleration (if positive) or deceleration (if negative) of the entire rock glacier within a year. Over the period of measurement, $\Delta\beta = 0$ on average. Figure 4 and Figure A5 in the Appendix illustrate the model fit. Among cryospheric sciences, this type of variance decomposition is mostly used in glaciology to analyze the distribution of mass balances on the glacier scale and mass-balance changes over time.[33,34,42–44] It is often referred to as the linear model. Two studies[45,46] have specifically applied this type of variance analysis to infer glacier kinetics as we have done in the present study for a rock glacier. The distribution of surface velocities in space and their variations over time (derived from Forbes' band locations) have been reconstructed at the Mer de Glace with this linear distribution model. In that particular case, it was effective in distinguishing

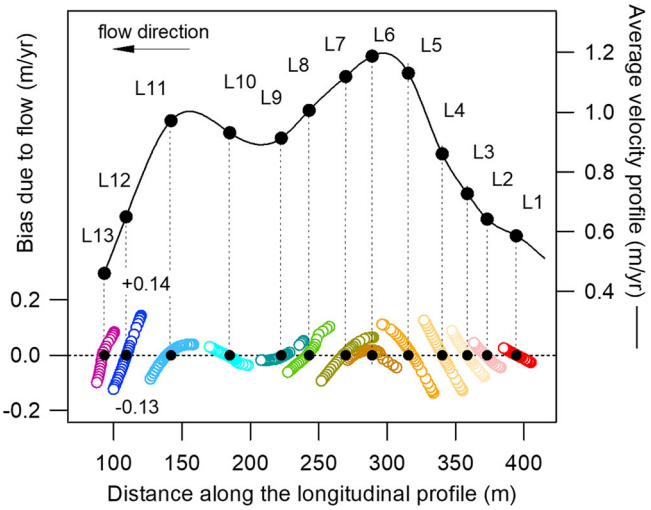

FIGURE 3 Average velocity profiles plotted according to the distance along the longitudinal profile (cubic spline black curve) and the associated bias affecting velocity changes due to block displacements. Open circles plot the annual velocity changes attributable to the travel of blocks during the recorded period. Biases are indicated for block L12 (see text) [Colour figure can be viewed at wileyonlinelibrary.com]

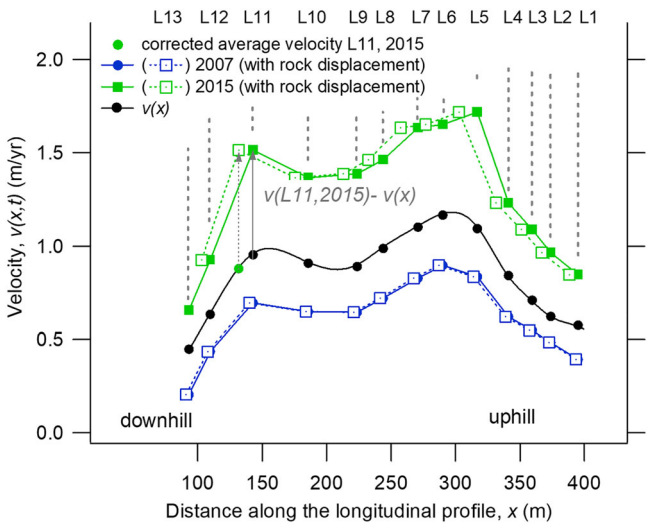

FIGURE 4 Surface velocity along the longitudinal profile in specific years (2007, 2015) to illustrate the annual deviations from the average velocity profile at each painted rock, $v(x)$, over the whole period of record (1983–2020). Dashed line profiles indicate rock displacements. For the specific year 2015, the deviation from the average is illustrated graphically with two arrows. The arrow with a dashed line shows the deviation with the (positive) correction due to block displacement. Block L13 disappeared from the longitudinal profile in 2015 (the profile has stopped at L12 since then) [Colour figure can be viewed at wileyonlinelibrary.com]

the time changes in velocity due to changes in ice flux from transverse changes in velocity due to friction and shear close to glacier margins. In our case, the spatial distribution of velocity is driven primarily by the slope along the longitudinal profile.

The second feature that can be identified in the upper and lower parts of the annual profiles is that the shift between annual profiles appears to be limited and a "compression" effect can be graphically observed at the profile endpoints, particularly for the blocks with the lowest velocities at the bottom of the profile (L12 and L13). This would appear to be a limitation for Equation (1) to adequately fit the data. To account for the larger velocity variations at the center of the profile compared to profile endpoints, an alternative to Equation (1) would then be to stipulate that the annual profiles are proportional to the average velocity profile, i.e.:

$$v(x,t) = \boldsymbol{v}(x)\Delta B(t) \quad (2)$$

where the time signal $\Delta B(t)$, similar to Equation (1), is a function of time alone and now denotes a dimensionless expansion/decrement factor of surface velocities with respect to the average profile. On average, $\Delta B(t) = 1$ over the period of observations, >1 on expansion, <1 on contraction and always positive. This formulation is referred to as the cross-coupling or cross-term model. It accounts for nonlinear effects in that the time response to the overall driving signal $\Delta B(t)$ is weighted by the local average velocity $\boldsymbol{v}(x)$. Figure A6 in the Appendix graphically illustrates this alternative fit.

We tested whether the linear (Equation 1) or the cross-term model (Equation 2) properly fit the data. To that end, the ability of Equations (1) and (2) to capture the data variability is analyzed with the residuals between the data and the functional form of both equations:

$$v(x,t) = \boldsymbol{v}(x) + \Delta\beta(t) + \varepsilon_\beta(x,t) \quad (3)$$

and:

$$v(x,t) = \boldsymbol{v}(x)\Delta B(t) + \varepsilon_B(x,t) \quad (4)$$

where the residuals ε_β and ε_B represent the variance unexplained by Equations (1) and (2), respectively, and corresponding to both measurement errors and discrepancies between the models and the data. The residuals ε are expected to have normal and centered distributions. For the models to be fully acceptable, the residuals should be on the order of the uncertainty of field measurements (±0.10 m/yr; section 3.1). In both cases, we used corrected values for $\boldsymbol{v}(x)$ to account for block displacements. Note that, in practice, the same inference scheme can be used for both models as in logarithm variables, i.e., Equation (2) become linear functional in form, $\log v(x,t) = \log \boldsymbol{v}(x) + \log \Delta B(t)$. Executable codes used for mass balance analyses can be loaded from, for example, https://glacioclim.osug.fr/Non-linear-model-for-mass-balance-calculation[44] to process the data.

4 | RESULTS

The results of the variance analysis are presented in Table 1. The variances explained by the decomposition according to Equations (2) and (2) are high (93 and 97%, respectively), showing that the adopted variance analysis models fit the data quite well and are well suited to the Laurichard rock glacier. This makes it possible to separately examine each model for spatial, temporal, and nonlinear effects, as well as residuals. The suitability of the variance models was checked using the standard Fisher–Snedecor F-test (variance comparison). Conducting statistical tests at the 95% confidence level, *p*-values are less than 10^{-5} for both models as obtained from F-ratio calculations (Table 1). Regarding residuals, ε_β and ε_B (Equations 3) and (4), their standard deviations (root mean square [RMS]) are in the range of the measurement errors with 11 and 8 cm/yr for the linear and cross-term models, respectively. The normality of their distributions was positively checked with the Kolmogorov–Smirnov test (D-test; Table 1).

4.1 | Spatial variability

The average velocity profile (mean velocity at each block versus the average block position; Figure 2b) shows the spatial structure of the velocity. The average velocity ranges from 0.2 to 1.2 m/yr, with maximum values in the steepest part of the profile (blocks L5–L7). This is typical of gravity-driven creep of ice or ice-rich debris mixtures with

TABLE 1 Variance captured by the two models, spatial and time variability, and variance of the data unexplained by the model. The common variance of the glacier-wide signals ($\Delta\beta(t)$, $\Delta B(t)$) with velocities of the painted rocks at the profile endpoints (L12, L13, L1, i.e., lowest velocity locations) is enhanced with the cross-term model. DF, degree of freedom for spatial and temporal variables, and for the unexplained factors (residuals); RMS, root mean square. K-S denotes the Kolmogorov–Smirnov test used for the residuals

	Δβ(*t*) linear model	**ΔB(*t*) cross-term model**
Overall variance of the data	0.35 m/yr	
Explained variance	93%	97%
Spatial variability of $\boldsymbol{v}(x)$	0.24 m/yr	0.25 m/yr
F-value (DF)	136.04 (12)	212.67 (12)
p-value	<0.00001	<0.00001
Time variability of $\Delta\beta(t)$, $\Delta B(t)$	0.25 m/yr	0.30 m/yr
F-value (DF)	70.65 (28)	113.83 (28)
p-value	<0.00001	<0.00001
RMS of the residuals (unexplained variance)	0.11 m/yr	0.08 m/yr
(DF)	(336)	(336)
K-S normality test		
D-value (DF)	0.0379 (376)	0.0704 (376)
p-value	0.773	0.125

maximum surface velocities just above the steepest slope area.[47] Minimal values are close to the rooting area at the top of the profile (L1) and at the rock glacier snout downstream (L12, L13).

The spatial variability (between painted blocks) of the data is the second source of variability (±0.24 m/yr) and is captured identically by both models. Differences in the average velocities between the different painted rocks along the longitudinal profile are significant, with deviations from the profile average exceeding the −100 to +100% range. This means that the sampling is well distributed along the flow line with respect to the spatial structure of the deformation. Additional painted rocks could be introduced between L4–L5 and L11–L12 because the differences in average velocities between the rocks of those two pairs (0.28 and 0.32 m/yr, respectively) exceed the overall spatial variability.

Given the separation of space and time variables in Equations (1) and (2), the mean rock glacier-wide velocity along the profile can be easily calculated, using, for example, simple arithmetic averaging:

$$v^* = \int_{L1}^{L13} v(x)dx = \frac{1}{13}\sum_{L1}^{L13} v(Li) \quad (5)$$

which produces an average surface velocity for the profile (all blocks) over the entire period of record of 0.86 m/yr with the linear model and 0.83 m/yr with the cross-term model. This average accounts for missing values as estimated by the variance analysis. A direct raw averaging (without any ANOVA) would overestimate the rock glacier-wide velocity as 0.89 m/yr due to missing values mainly at blocks of low velocity (L2 at the beginning of the series and L13 since 2015).

4.2 | Time variability

With a slightly higher explained variance provided by Equation (2) for the cross-term model, $\Delta B(t)$ better captures the time signal accounting for low velocity responses on locations in the upper and bottom parts of the profile (Table 1). The temporal (year-to-year) variability is the main source of variability in the data, with ±0.25 m/yr as captured by the linear model, and ±0.30 m/yr by the cross-term model. This is shown by large scattering of the annual colored profiles in Figure 2b. For some years (e.g., 1999, 2015, 2019, 2020) velocities can reach up to 2 m/yr and these accelerations are observed all along the profile of velocities that are shifted up by approximately the same amount at each block. Conversely, strong and general decelerations (in the 1980s, 2006, 2007) reduce velocities to 0.3–0.7 m/yr for all blocks along the profile. Equation (2) performs slightly better in capturing the time variability at the ends of the profile where the year to year velocity changes are attenuated compared to the profile center. The temporal source of changes in the surface velocity is the first source of variability in the data and is a strong effect when compared to the velocity distribution along the longitudinal profile. This time response is well captured by Equations (1) and (2) because there is a strong decoupling between spatial and temporal dependences.

Despite their differences, both equations retrieve from the data two time signals for velocity changes that are in very close agreement and highly correlated ($\rho^2 = 0.99$). They both exhibit a long-term trend of acceleration from the mid-1980s to the present, but with a slower period from 1999 to the mid-2000s (Figure 5). From 1983 to 1997, velocities were lower than the long-term average (common line $\Delta\beta(t) = 0$ and $\Delta B(t) = 1$) with a minimum velocity around 1985–86 (0.4 m/yr). The next period, 1998–2010, was almost in line with the long-term average (around 0.85 m/yr), though slightly higher in the early 2000s and lower in the late 2000s. Then from 2010 to 2020, velocities significantly increased with a maximum in 2020 (1.55 m/yr). Therefore, two phases of acceleration can be identified from the mid-1980s to 1999 and from 2007 to 2020. Those two periods were interrupted by the 1997–2005 period of almost steady-state velocities. This feature is confirmed with velocity analyses derived from aerial images over the larger time span 1952–2020.[27]

4.3 | Residuals

The residuals have normal and centered distributions (Figure 6). The variance (RMS) of residuals is indicated in Table 1. Again, comparing overall residuals for both models shows that the cross-term model fits the data better, with a residual of ±8 cm/yr compared to ±11 cm/yr for the linear model. Residuals at individual block locations range between 0.05 and 0.43 m/yr. The high latter value (block L5 in 2016) can be considered as an outlier due to tilting or sliding on the steep slope where this block is located, or a gross measurement error. Nevertheless, such high values are infrequent, as suggested by the distribution of residuals exhibited in Figure 6.

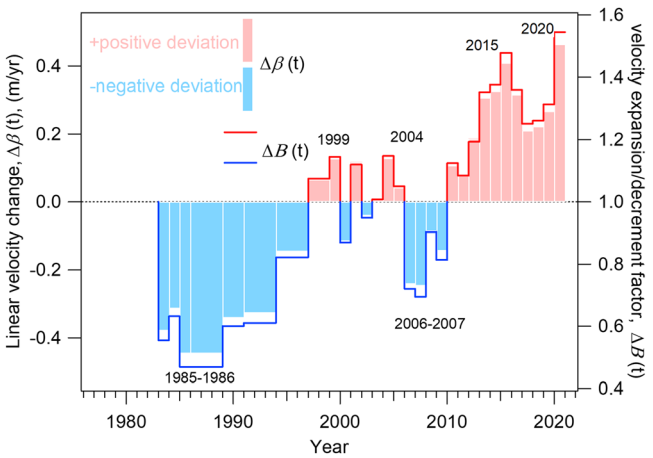

FIGURE 5 Velocity changes between 1984 and 2020. Linear, $\Delta\beta(t)$, and cross-term, $\Delta B(t)$, velocity changes resulting from the two variance-decomposition models (Equations (1) and (2)) and representing the common time response (glacier-wide) at all measurement points. This time signal provides the best possible estimate of the glacier-wide response in surface velocity to the external drivers [Colour figure can be viewed at wileyonlinelibrary.com]

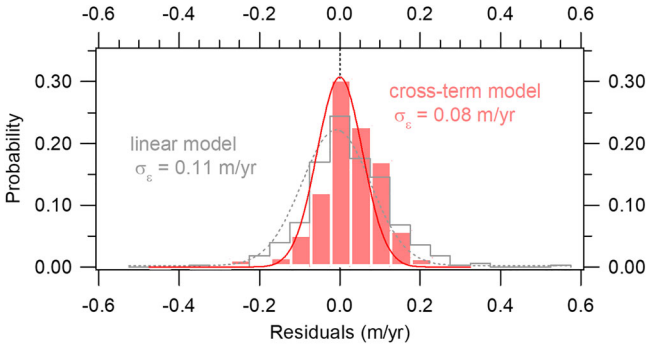

FIGURE 6 Distribution of the residuals for the two models [Colour figure can be viewed at wileyonlinelibrary.com]

Analysis of the residual time series did not reveal a time correlation ($r^2 = 0.22$), as shown in Figure A7 in the Appendix, and no trend was detectable over the period of record. Note that in Figure A7, it would appear that the cross-term model performs better than the linear model in the first 5 years of the record with significantly lower residuals. This is probably due to the low velocities encountered over that period during which nonlinear effects were more frequent. Spatially, the cross-term model performs better than the linear model at the ends of the profile (L1, L12, L13) where lower residuals were produced (6, 10, and 8 cm/yr, respectively, compared to 13, 11, and 12 cm/yr).

For the models to be fully acceptable, the residuals must be compared with measurement errors (here ±0.10 m/yr). The standard deviation of the residuals (Table 1) is virtually equal (linear model) or slightly lower (cross-term model) than the uncertainty of the field measurements. As the difference between the residual variance and the measurement variance can be considered a rough estimate of the model error, this indicates that both models fit the data well.

4.4 | Validation at transverse profile O

Surface velocities recorded along the transverse profile O can be used as independent data to validate the time signal provided by the two models. We calculated velocity changes at blocks O3–O7 between 2008 and 2020 (other blocks unfortunately have missing values for some years). The scatter plot in Figure 7 shows the correlation between the 12 year-to-year velocity changes at these five blocks with the time signal of the linear model. The correlation is high and is better for the blocks at the central locations (O4– O6) which are close to blocks L11 and L12. The best correlations are observed for the blocks with the highest velocities (O4, O5). The lowest correlation is for block O7, which has the lowest average velocity over the period 2008–2020. For all blocks of the O profile, residuals between observed velocity changes and $\Delta\beta$ are between 8 and 10 cm/yr, which is approximately equal to the margin of error for measurements. Similar (not significantly different) results are obtained for the cross-term model (data not shown). This analysis confirms that both models

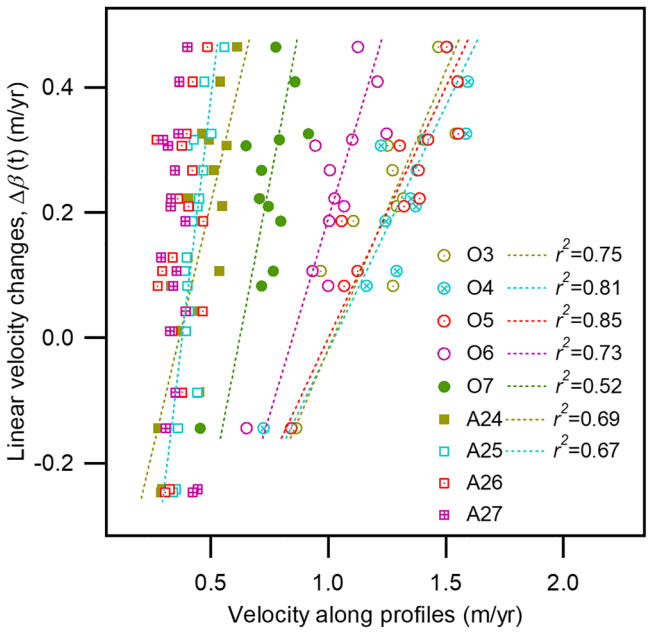

FIGURE 7 Scatter plot of velocity changes observed on profiles A and O, and time changes in velocity captured by the linear model. [Colour figure can be viewed at wileyonlinelibrary.com]

provide a time signal that has a rock glacier-wide significance. However, the cross-model performs better at locations of low velocity (i.e., on gentle slopes), along the rock glacier margins, and at profile endpoints. Similar conclusions can be drawn from observations at profile A (Figure 7), but to a lesser extent because velocities are lower at the rock glacier rooting area, not exceeding more than 0.5 m/yr.

5 | DISCUSSION

In this study, we retrieved the time changes in velocities from a variance analysis well suited to differentiate spatial and time variabilities that are almost of the same order of magnitude at Laurichard rock glacier (0.25–0.3 m/yr). Time changes are the major factor in variability being slightly greater than the spatial factor. Extracting the time signal is nevertheless possible because the year-to-year variation is decoupled from the spatial structure of the velocity. Therefore, acceleration and deceleration are virtually the same over the entire rock glacier surface. The linear model fits the data quite well, explaining 93% of the data variability. Approximately 10% of the variance is unexplained by the linear model, but that corresponds roughly to the margin of error in measurements. Nonlinear effects are second-order effects arising mainly at locations characterized by low velocity (notably at the rock glacier root and snout) and by limited slope, where homothetic changes mostly occur (i.e., proportional to the local velocity). This explains why the cross-model performs slightly better in capturing those attenuated velocity variations, with 97% explained variance, and lower residuals.

In light of the fit of the two models, the spatial structure of velocity has remained almost unchanged over the three decades of record

and can be considered steady. Annual deviations from this average steady-state flow/creep structure are almost uniform spatially except at locations characterized by very low displacements where nonlinear effects occur.

5.1 | Potential processes driving velocity time changes

Although the mechanical processes further, for instance with ad hoc rheology for the creeping material,[48,49] is beyond the scope of this paper, some qualitative information can nevertheless be deduced from the time response and the spatial distribution of velocity.

The process of velocity changes with rock glacier-wide overall accelerations/decelerations suggests that the rock glacier might behave like a bulk sliding-block with changing sliding or creep conditions occurring on a large scale. Uniform changes in velocity suggest that acceleration or deceleration are not particularly dependent on local rock glacier features (e.g., slope) or ice content. It also suggests that the process is rather a surface process located at a slip or highly sheared interface affecting the rock glacier as a whole. Such processes have already been proposed to explain rock-glacier destabilization.[11,50]

Alternatively, the nonlinear effects, mainly detectable at the rock glacier margins, suggest that velocity changes are also related to rheology changes within the bulk ice/ice-rich body with creep variations caused by changes in the apparent softness of the rock glacier material. In cases of gravity-driven creep (e.g., for nonlinear viscous material[47]) the surface velocity is expected to change homothetically through the activation of the so-called A rate factor of the constitutive law describing the softness of the rock glacier material (e.g., for pure polycrystalline ice[51]; see also[20]). Adopting $n = 3$ in Glen's law, the surface velocity from internal deformation V_s over thickness H is given by[52]:

$$V_s = \frac{1}{2}A\left(\rho g \frac{dH}{dx}\right)^3 H^4 \tag{6}$$

where dH/dx is the surface slope, ρ is the ice density and g the acceleration due to gravity. A is the (inverse) viscosity rate factor depending in particular on temperature (for ice below the melting point) through an Arrhenius-type temperature dependence:

$$A = A_0 e^{-\frac{Q}{RT}} \tag{7}$$

where A_0 is a constant independent of temperature, R is the universal perfect gas constant (8.314 kJ/mol), Q the creep-activation energy of the ice, and T the absolute temperature of the ice.

Qualitatively, the functional form of the cross-term model (Equation 2) is inherently consistent with Equation (6), and expected velocity changes associated with variations in the A rate factor are consistent with temperature changes. Such a constitutive relationship has already been applied and discussed in other studies on rock glacier creep (e.g.,[20,49,53–56]) as well as laboratory experiments dedicated to mechanical creep tests.[48,57] Quantitatively, using the average velocity recorded at block L8 (central location, 1 m/yr) and the local rock glacier geometry ($H \sim 20$ m, $dH/dx = 0.6$[26,36]) in the median steepest part of the rock glacier results in a value of $A = 0.8 \times 10^{-16}$ $(\text{Pa})^{-3}\ \text{yr}^{-1}$. This corresponds to values ($0.8–1.5 \times 10^{-16}$ $(\text{Pa})^{-3}\ \text{yr}^{-1}$) reported for pure ice between -2 and 0°C.[47,58–60]

Regarding observed changes in velocity at Laurichard rock glacier, the velocity factor $\Delta B(t)$ of Equation (2) varies by a factor of $\alpha = 3.14$ between 1986 and 2015 (Figure 5). If we accept that a change in ice temperature is the process driving the increase in surface velocities due to the A factor according to Equation (6), such a velocity change is explainable by a temperature increase ΔT derived from Equation (7):

$$\Delta T = \frac{RT(T+\Delta T)}{Q} ln\alpha \cong \frac{RT^2}{Q} ln\alpha \tag{8}$$

Fixing a creep-activation energy of 139 kJ/mol in the temperature range -8 to -2°C,[61] a temperature change of $\Delta T = +4.8$°C is needed. This simple calculation shows that temperature is probably not the only factor responsible for activating the creep change. Such a rise in internal temperature seems unlikely: it would first require an initial temperature of -5°C or lower as the ice temperature is upper bounded by the melting point. Furthermore, the calculated temperature rise (+1.3°C per decade) is high compared to atmospheric-warming data from weather stations (0.83°C per decade since 1983 at Besse Météo-France, 18 km distant), from homogenized records (HISTALP,[62]), and from englacial temperatures[63] which report trends in the range of 0.3–0.5°C per decade.

Moreover, the time needed for a thermal conduction wave to diffuse through the thickness of the rock glacier would delay the internal warming substantially. The temperature change $\Delta T(d,t)$ at depth d after a time t following an increment of temperature at the surface ΔT_s is given by the error function, erf[64]:

$$\Delta T(d,t) = \Delta T_s\left[1 - \text{erf}\left(\frac{d}{2\sqrt{Dt}}\right)\right] \tag{9}$$

where D is the thermal diffusion of ice and/or granite (1.2×10^{-6} m^2/s). As an illustration of the slow process of Equation (9), the time needed for ΔT to reach 70% of ΔT_s is given by $\text{erf}\left(d/\left(2\sqrt{Dt}\right)\right) = 0.3$, which requires roughly $d/\left(2\sqrt{Dt}\right) = 0.25$. This results in a time delay t of 50 years at a depth of $d = 20$ m and 10 years at $d = 10$ m. This simple calculation shows that thermal diffusion cannot alone explain the thermal activation (via the inverse viscosity A factor) at annual time steps through the bulk rock glacier body. Thermal creep-activation, if involved, is therefore not the single process.

Other processes may therefore explain year-to-year changes, for instance a change in the liquid water content at ice-grain boundaries if ice is at the melting point. Ice viscosity is indeed very sensitive to water content.[65–67] The A factor is reported to increase by a factor of 4–5 when the liquid-water content increases from 0 to 0.8%.[67] This

single process would increase surface velocities greatly, given that they are proportional to A (Equation 6). Lliboutry[68] analyzed such a process of positive feedback, leading to possible instability in temperate glaciers because the dissipation of energy due to higher creep rates produces additional meltwater, and hence an even lower viscosity. Furthermore, enhanced creep rates should increase friction processes between ice and debris, dissipating more heat acting as an additional energy source for ice to melt.

On the larger scale of the bulk ice–debris mixture of the rock-glacier body, processes including rain and meltwater circulation, and effective pressure at the sliding/sheared basal interface have also been proposed.[14,21] Other processes not calling on liquid water, such as fractures or deformation of subglacial debris, have also been proposed.[11] However, despite qualitative and quantitative factors indicating links between the data and the above elementary processes that may drive the flow of the Laurichard rock glacier, it is beyond the scope of this paper to draw firm conclusions about which processes effectively rule the dynamics at Laurichard rock glacier.

5.2 | Rock glacier average-wide velocity

In search of a spatial average of velocity changes at the glacier scale, we retain the cross-term model (Equation 2) to provide the time series of velocity changes because it explains much of the data variability. At the same time and as discussed above, it provides an understandable framework in qualitative agreement with ice creep and rock glacier flow and their control by an association of changes in ice temperature and liquid water.

In practice, the time–space variability separation of Equation (2) also makes it possible to easily calculate an annual rock glacier-wide velocity, $\overline{\boldsymbol{v}(t)}$, because the time function $\Delta B(t)$ is decoupled from the spatial dependence and its averaging. Adopting simple arithmetic averaging, this results in:

$$\overline{\boldsymbol{v}}(t) = \int_{L1}^{L13} v(x,t)dx = \int_{L1}^{L13} \boldsymbol{v}(x)\Delta B(t)dx = \boldsymbol{v}^* \Delta B(t) \qquad (10)$$

for the cross-term model. This shows that the annual velocity for the whole rock glacier is simply an increment/decrement with respect to the long-term average of the velocity profile $\boldsymbol{v}^*$ given by Equation (5) and illustrated in Figure 8. It provides a time signal that is not affected by missing values (blocks not measured in some years). Using instead a simple average of all measured velocities in each year would result in a time signal affected by an error of up to 10%. This is due to missing values whose absence skews the average up or down depending on whether they are above or below the overall average (Figure 8). These biases are significant only in the last years of the series, exceeding the confidence interface of $\boldsymbol{v}^* \Delta B(t)$. A variance decomposition is therefore recommended to provide a signal of velocity changes on the rock glacier scale. Year-to-year variability is also made less evident by direct averaging of the entire dataset (±0.25 compared to ±0.30 m/yr) and use of a variance analysis is also recommended for this purpose.

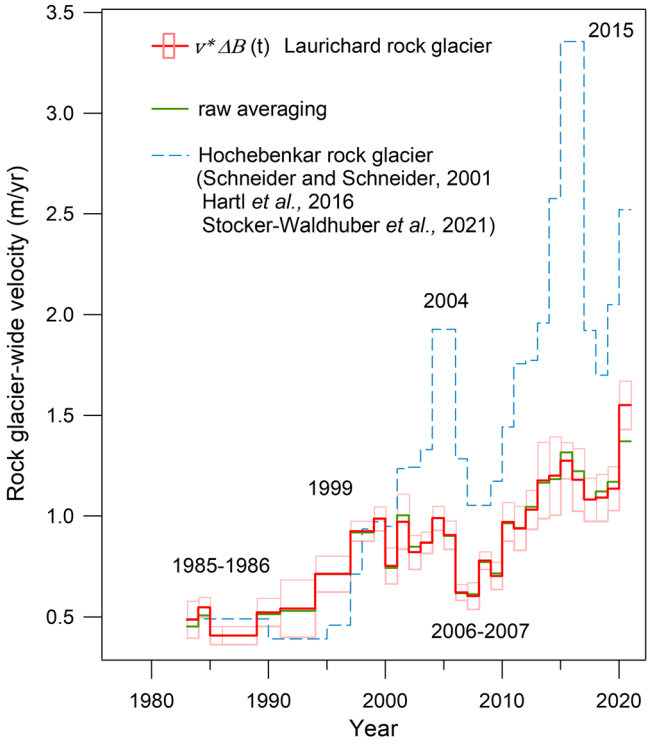

FIGURE 8 Rock glacier-wide velocity changes between 1984 and 2020 at Laurichard rock glacier. This overall velocity signal is given by the simple product of the time signal $\Delta B(t)$ and the average velocity along the profile $\boldsymbol{v}^*$. Pink boxes show the 95% confidence interval (±2σ residuals). Raw averaging is a direct calculation without any ANOVA. The blue dashed line is the velocity time plot for the Hochebenkar rock glacier (Austria) [Colour figure can be viewed at wileyonlinelibrary.com]

Furthermore, measurement errors (outliers) can be detected by the variance analysis, by searching for large residuals or large discrepancies between velocity changes at point locations compared to the overall variance. Equation (10) provides a velocity signal that is easily comparable to other velocity changes retrieved from other rock glaciers for joint analyses (e.g.,[9]; Figure 8, Hochebenkar rock glacier). The dimensionless signal, $\Delta B(t)$, which does not depend on the adopted velocity averaging, can be linked to co-variables in searching for driving factors such as weather conditions and seasonal snow cover.

6 | CONCLUSION

The surface velocities recorded at the Laurichard rock glacier since 1984 are an exceptional data series, spanning more than three decades, and revealing changes in the creep kinematics of this peculiar, ice-rich, permafrost landform. From our analyses, one see that:

- Change in velocity is essentially a homogeneous process at the rock glacier scale. This means that annual accelerations or decelerations as well as long-term trends are virtually identical over the entire rock glacier surface. Nonlinear processes in velocity changes

occur punctually at very low-velocity locations, close to the rock glacier margins. At those points, velocity changes tend instead to be proportional to the local velocity.

- The time signal extracted by the variance analysis provides a rock glacier-wide signal. We would recommend using one of the two ANOVA models to retrieve a velocity signal relevant at the rock glacier scale. As used in the glaciological community, a glacier-wide mass balance is now commonly used to characterize the glacier response to climate change and is routinely published by the World Glacier Monitoring Service (WGMS; https://wgms.ch/).
- The spatial structure of surface velocity has been in steady state for over four decades. The spatial structure of velocity changes (acceleration/deceleration as a block) suggests that it is driven by a wide-acting process, acting at the overall rock glacier scale.
- The process of internal increases in ice temperatures alone (and associated changes in creep rates) would seem insufficient to explain the long-term rise of surface velocities and their annual variations. Changes in the liquid-water is a possible contributory factor, due to the injection of seasonal water caused by melting snow cover or internal melt due to heat generated by enhanced ice creep and friction in the ice-debris mixture. Further studies using Laurichard rock glacier surface velocities may focus on the dynamics based on preliminary studies dedicated to the material rheology (e.g.,[49]) given that the geometry of the rock glacier is now better constrained.[36]

FUNDING STATEMENT

The last two decades of the survey were supported by CryobsClim "Long-term Observation and Experimentation System for Environmental Research" (SOERE/All'envi) and the PermaFrance observatory "monitoring mountain permafrost in the French Alps." The Ecrins National Park is warmly thanked for its support in funding and helping field surveys since the early 2000s. INRAE is a part of Labex@Osug2020.

CONFLICT OF INTEREST DISCLOSURE

The authors declare they have no conflicts of interest.

ACKNOWLEDGEMENTS

We thank B. Francou and L. Reynaud who initiated the survey in 1979 and performed the early measurements of the series (1983–2000) with C. Vincent (IGE, CNRS-UGA). Field measurements were then carried out by E. Thibert (Ecrins National Park and later ETNA, INRAE-UGA), from 2001 to the present with M. Bouvier (Ecrins National Park) and Mylène Bonnefoy-Demongeot (INRAE-UGA). The last two decades of the survey were supported by CryobsClim "Long-term Observation and Experimentation System for Environmental Research" (SOERE/All'envi) and the PermaFrance observatory "monitoring mountain permafrost in the French Alps" with support from OSUG. Ecrins National Park is warmly thanked for its support in funding and helping field surveys since the early 2000s. INRAE is a part of Labex@OSUG2020. The authors are grateful to the editor Pr. M. Guglielmin and three anonymous reviewers whose comments and suggestions improved the clarity of the manuscript.

DATA AVAILABILITY STATEMENT

Velocity data are given in the Supporting Information. Raw positioning data are available from the corresponding author upon request.

ORCID

Emmanuel Thibert https://orcid.org/0000-0003-2843-5367
Xavier Bodin https://orcid.org/0000-0001-6245-4030

REFERENCES

1. Haeberli W. *Creep of Mountain Permafrost: Internal Structure and Flow of Alpine Rock Glaciers*. Zürich: Mitteilungen der VAW, ETH; 1985:142.
2. Hock R, Rasul G, Adler C, et al. High Mountain Areas Supplementary Material. In: Pörtner H-O, Roberts DC, Masson-Delmotte V, et al., eds. *IPCC Special Report on the Ocean and Cryosphere in a Changing Climate*. Cambridge, UK and New York, NY, USA: Cambridge University Press; 2019:131-202. doi:10.1017/9781009157964.004
3. Buchli T, Kos A, Limpach P, Merz K, Zhou X, Springman SM. Kinematic investigations on the Furggwanghorn Rock Glacier, Switzerland. *Permafr Periglac Process*. 2018;29(1):3-20. doi:10.1002/ppp.1968
4. Kenner R, Pruessner L, Beutel J, Limpach P, Phillips M. How rock glacier hydrology, deformation velocities and ground temperatures interact: Examples from the Swiss Alps. *Permafr Periglac Process*. 2020;31(1):3-14. doi:10.1002/ppp.2023
5. Bodin X, Schoeneich P, Deline P, et al. Mountain permafrost and associated geomorphological processes: recent changes in the French Alps. *J Alpine Res*. 2015;103-2(103-2). doi:10.4000/rga.2885
6. Delaloye R, Morard S, Barboux C, et al. In: Graf C, ed. *Rapidly moving rock glaciers in Mattertal*. Jahrestagung der Schweizerischen Geomorphologischen Gesellschaft; 2013:21-31.
7. Delaloye R, Perruchoud E, Avian M, et al. Recent Interannual Variations of Rockglaciers Creep in the European Alps. Proceedings of the Ninth International Conference on Permafrost, Fairbanks, USA, June; 2008:343-348.
8. Gärtner-Roer I, Avian M, Delaloye R, et al. Rockglacier speed-up throughout European Alps-a climatic signal. Proceedings of the second European conference on permafrost, Potsdam, German, 12–16 June 2005; 2005:101-102.
9. Kellerer-Pirklbauer A, Delaloye R, Lambiel C, et al. Interannual variability of rock glacier flow velocities in the European Alps. Proceedings of the 5th EUROPEAN CONFERENCE ON PERMAFROST, Chamonix, France, 23 June-1st July 2018; 2018;396-397.
10. Bodin X, Krysiecki JM, Schoeneich P, et al. The 2006 Collapse of the Bérard Rock Glacier (Southern French Alps). *Permafr Periglac Process*. 2016;2(1):209-223. doi:10.1002/ppp.1887
11. Marcer M, Serrano C, Brenning A, Bodin X, Goetz J, Schoeneich P. Evaluating the destabilization susceptibility of active rock glaciers in the French Alps. *Cryosphere*. 2019;13(1):141-155. doi:10.5194/tc-13-141-2019
12. Micheletti N, Lambiel C, Lane SN. Investigating decadal-scale geomorphic dynamics in an alpine mountain setting. *J Geophys Res Earth*. 2015;120(10):2155-2175. doi:10.1002/2015JF003656
13. Roer I, Haeberli W, Avian M, et al. Observations and considerations on destabilizing active rock glaciers in the European Alps. In: 9th International Conference on Permafrost, Fairbanks, Alaska, 29 June 2008–3 July 2008; 2008:1505-1510.

14. Cicoira A, Beutel J, Faillettaz J, Vieli A. Water controls the seasonal rhythm of rock glacier flow. *Earth Planet Sci Lett*. 2019;528:115844. doi:10.1016/j.epsl.2019.115844
15. Delaloye R, Lambiel C, Gärtner-Roer I. Overview of rock glacier kinematics research in the Swiss Alps. *Geographica Helvetica*. 2010;65(2):135-145. doi:10.5194/gh-65-135-2010
16. Ikeda A, Matsuoka N. Degradation of talus-derived rock glaciers in the Upper Engadin, Swiss Alps. *Permafr Periglac Process*. 2002;13(2):145-161. doi:10.1002/ppp.413
17. Marcer M, Cicoira A, Cusicanqui D, et al. Rock glaciers throughout the French Alps accelerated and destabilised since 1990 as air temperatures increased. *Commun Earth Environ*. 2021;2(1):81. doi:10.1038/s43247-021-00150-6
18. Roer I, Kääb A, Dikau R. Rockglacier acceleration in the Turtmann valley (Swiss Alps): Probable controls. *Norsk Geografisk Tidsskrift-Norwegian J Geogr*. 2005;59(2):157-163. doi:10.1080/00291950510020655
19. Springman SM, Arenson LU, Yamamoto Y, et al. Multidisciplinary investigations on three rockglaciers in the Swiss Alps: Legacies and future perspectives. *Geogr Ann Ser B*. 2012;94(2):215-243. doi:10.1111/j.1468-0459.2012.00464.x
20. Kääb A, Frauenfelder R, Roer I. On the response of rockglacier creep to surface temperature increase: Climate Change Impacts on Mountain Glaciers and Permafrost. *Global Planet Change*. 2007;56(1-2):172-187. doi:10.1016/j.gloplacha.2006.07.005
21. Wirz V, Gruber S, Purves RS, et al. Short-term velocity variations of three rock glaciers and their relationship with meteorological conditions. *Earth Surf Dyn*. 2016;4(1):103-123. doi:10.5194/esurf-4-103-2016
22. Ikeda A, Matsuoka N, Kääb A. Fast deformation of perennially frozen debris in a warm rock glacier in the Swiss Alps: an effect of liquid water. *J Geophys Res*. 2008;113(F01021):2156-2202. doi:10.1029/2007JF000859
23. Hartl L, Fischer A, Stocker-Waldhuber M, Abermann J. Recent speed-up of an alpine rock glacier: an updated chronology of the kinematics of outer hochebenkar rock glacier based on geodetic measurements. *Geogr Ann Ser B*. 2016;98(2):129-141. doi:10.1111/geoa.12127
24. Schneider B, Schneider H. Zur 60jährigen Messreihe der kurzfristigen Geschwindigkeitsschwankungen am Blockgletscher im Äusseren Hochebenkar, Ötztaler Alpen, Tirol. *Zeitschrift für Gletscherkunde Und Glazialgeologie*. 2001;37(1):1-33.
25. Staub B, Marmy A, Hauck C, Hilbich C, Delaloye R. Ground temperature variations in a talus slope influenced by permafrost: a comparison of field observations and model simulations. *Geographica Helvetica*. 2015;70(1):45-62. doi:10.5194/gh-70-45-2015
26. Bodin X, Thibert E, Sanchez O, Rabatel A, Jaillet S. Multi-annual Kinematics of an Active Rock Glacier Quantified from Very High-Resolution DEMs: An Application-Case in the French Alps. *Remote Sens (Basel)*. 2018;10(4):547. doi:10.3390/rs10040547
27. Cusicanqui D, Rabatel A, Vincent C, Bodin X, Thibert E, Francou B. Interpretation of volume and flux changes of the Laurichard rock glacier between 1952 and 2019. *J Geophys Res*. 2021;129(9):e2021JF006161. doi:10.1029/2021JF006161
28. Eriksen HØ, Rouyet L, Lauknes TR, et al. Recent acceleration of a rock glacier complex, Adjet, Norway, documented by 62 years of remote sensing observations. *Geophys Res Lett*. 2018;45(16):8314-8323. doi:10.1029/2018GL077605
29. Haeberli W, Hallet B, Arenson L, et al. Permafrost creep and rock glacier dynamics. *Permafr Periglac Process*. 2006;17(3):189-214. doi:10.1002/ppp.561
30. Kääb A. Remote sensing of permafrost-related problems and hazards. *Permafr Periglac Process*. 2008;19(2):107-136. doi:10.1002/ppp.619
31. Vivero S, Lambiel C. Monitoring the crisis of a rock glacier with repeated UAV surveys. *Geographica Helvetica*. 2019;74(1):59-69. doi:10.5194/gh-74-59-2019
32. Stocker-Waldhuber M, Fischer A, Hartl L, Abermann J, Schneider H. Flow velocity records at Rock Glacier Outer Hochebenkar (Äußeres Hochebenkar), Ötztal, Tyrolian Alps, Austria, 1997 et seq.. *PANGAEA*. 2021. doi:10.1594/PANGAEA.928244
33. Eckert N, Baya H, Thibert E, Vincent C. Extracting the temporal signal from a winter and summer mass-balance series: application to a six-decade record at Glacier de Sarennes, French Alps. *J Glaciol*. 2011;57(201):134-150. doi:10.3189/002214311795306673
34. Lliboutry L. Multivariate statistical analysis of glacier annual balances. *J Glaciol*. 1974;13(69):371-392. doi:10.3189/S0022143000023169
35. Francou B, Reynaud L. Ten years of surficial velocities on a rock glacier (Laurichard, French Alps). *Permafr Periglac Process*. 1992;3(3):209-213. doi:10.1002/ppp.3430030306
36. Guillemot A, Baillet L, Garambois S, et al. Modal sensitivity of rock glaciers to elastic changes from spectral seismic noise monitoring and modelling. *The Cryosphere*. 2021;15:509-521. doi:10.5194/tc-15-501-2021
37. Bodin X, Thibert E, Fabre D, et al. Two Decades of Responses (1986–2006) to Climate by the Laurichard Rock Glacier, French Alps. *Permafr Periglac Process*. 2009;20(4):331-344. doi:10.1002/ppp.665
38. Durand Y, Giraud G, Laternser M, Etchevers P, Mérindol L, Lesaffre B. Reanalysis of 47 Years of Climate in the French Alps (1958–2005): Climatology and Trends for Snow Cover. *J Appl Meteorol Climatol*. 2009;48(12):2487-2512. doi:10.1175/2009JAMC1810.1
39. Durand Y, Laternser M, Giraud G, Etchevers P, Lesaffre B, Mérindol L. Reanalysis of 44 Years of Climate in the French Alps (1958–2002): Methodology, Model Validation, Climatology, and Trends for Air Temperature and Precipitation. *J Appl Meteorol Climatol*. 2009;48(3):429-449. doi:10.1175/2008JAMC1808.1
40. Francou B. *Géodynamique des éboulis et formes associées de la Combe de Laurichard*. Grenoble: Université Joseph Fourier; 1981 PhD: 153.
41. Bevington PR. *Data reduction and error analysis for the physical sciences*. New York: McGraw-Hill; 1969.
42. Rasmussen LA. Altitude variation of glacier mass balance in Scandinavia. *Geophys Res Lett*. 2004;31(13):L13401. doi:10.1029/2004GL020273
43. Thibert E, Vincent C. Best possible estimation of mass balance combining glaciological and geodetic methods. *Ann Glaciol*. 2009;50(50):112-118. doi:10.3189/172756409787769546
44. Vincent C, Soruco A, Azam MF, et al. A nonlinear statistical model for extracting a climatic signal from glacier mass balance measurements. *J Geophys Res*. 2018;123(9):2228-2242. doi:10.1029/2018JF004702
45. Lliboutry L, Reynaud L. "Global Dynamics" of a temperate valley glacier, Mer de Glace, and past velocities deduced from Forbes'bands. *J Glaciol*. 1981;27(96):207-226. doi:10.3189/S0022143000015367
46. Reynaud L. Reconstruction of past velocities of Mer de Glace using Forbes'bands. *Zeitschrift für Gletscherkunde Und Glazialgeologie*. 1979;15(2):149-163.
47. Paterson WSB. *The physics of glaciers*. 3rded. Oxford (UK): Butterworth-Heinemann; 1994. doi:10.1016/C2009-0-14802-X.
48. Arenson LU, Springman SM. Mathematical descriptions for the behaviour of ice-rich frozen soils at temperatures close to 0°C. *Can Geotech J*. 2005;42(2):431-442. doi:10.1139/t04-109
49. Melki S, Daudon D, Bodin X, Thibert E. Analysis of the Mechanical Behavior of the Laurichard Rock Glacier (French Alps) in the Recent Climatic Changes. In: Barla M, Di Donna A, Sterpi D, eds. *Challenges and Innovations in Geomechanics*. Proceedings of the 16th International Conference of IACMAG-Volume 2 (Lecture Notes in Civil Engineering Book 126). Berlin: Springer; 2021. doi:10.1007/978-3-030-64518-2_109.
50. Lambiel, C. Le glacier rocheux déstabilisé de Tsaté-Moiry (VS) caractéristiques morphologiques et vitesses de déplacement. In: *La géomorphologie alpine: Entre patrimoine et contrainte/actes du colloque de la Société suisse de géomorphologie*. 3–5 September 2009, Olivone. Géovisions, 36, Institut de géographie de l'Univ. de Lausanne, Lausanne; 2011:211-224.

51. Glen JW. The creep of polycristalline ice. *Proc Royal Soc A*. 1955; 228(1175):519-538. doi:10.1098/rspa.1955.0066
52. Lliboutry L. A critical review of analytical approximate solutions for steady state velocities and temperatures in cold ice-sheets. *Zeitschrift für Gletscherkunde Und Glazialgeologie*. 1979;35(2): 135-148.
53. Barsch D. Permafrost Creep and Rockglaciers. *Permafr Periglac Process*. 1992;3(3):175-188. doi:10.1002/ppp.3430030303
54. Frauenfelder R, Schneider B, Kääb A. Using dynamic modelling to simulate the distribution of rockglaciers. *Geomorphology*. 2008;93(1-2): 130-143. doi:10.1016/j.geomorph.2006.12.023
55. Müller J, Vieli A, Gärtner-Roer. Rock glaciers on the run – understanding rock glacier landform evolution and recent changes from numerical flow modelling. *Cryosphere*. 2016;10(6):2865-2886. doi:10.5194/tc-10-2865-2016
56. Whalley W, Azizi F. Rheological models of active rock glaciers – Evaluation, Critique and a possible test. *Permafr Periglac Process*. 1994; 5(1):37-51. doi:10.1002/ppp.3430050105
57. Arenson LU, Johansen MM, Springman SM. Effects of volumetric ice content and strain rate on shear strength under triaxial conditions for frozen soil samples. *Permafr Periglac Process*. 2004;15(3):261-271. doi:10.1002/ppp.498
58. Budd WF, Jacka TH. A review of ice viscosity for ice sheet modelling. *Cold Reg Sci Technol*. 1989;16(2):116-144. doi:10.1016/0165-232X(89)90014-1
59. Morgan VI. High temperature ice creep tests. *Cold Reg Sci Technol*. 1991;19(3):295-300. doi:10.1016/0165-232X(91)90044-H
60. Raymond CF. Valley glaciers. In: Colbeck CS, ed. *Dynamics of Snow and Ice Masses*. New-York: Academic Press; 1980:79-139. doi:10.1016/B978-0-12-179450-7.50007-3.
61. Weertman J. Creep of ice. In: Whalley E, Jones SJ, Gold LW, eds. *Physics and Chemistry of ice*. Royal Society of Canada (Ottawa); 1973: 320-337.
62. Chimani B, Matulla C, Böhm R, Hofstätter M. A new high resolution absolute Temperature Grid for the Greater Alpine Region back to 1780. *Int J Climatol*. 2013;33(9):2129-2141. doi:10.1002/joc.3574
63. Gilbert A, Vincent C. Atmospheric temperature changes over the 20th century at very high elevations in the European Alps from englacial temperatures. *Geophys Res Lett*. 2013;40(10):2102-2108. doi:10.1002/grl.50401
64. Carslaw HS, Jaeger JC. *Conduction of Heat in Solids*. 2nded. Oxford (UK): Oxford University Press; 1986.
65. Barnes P, Tabor D, Walker JCF. The friction and creep of polycrystalline ice. *Proc R Soc A: Math Phys Eng Sci*. 1971;324:127-155. doi:10.1098/rspa.1971.0132
66. de La Chapelle S, Milsh H, Castelneau O, Duval P. Compressive creep of ice containing a liquid intergranular phase: rate controlling processes in the dislocation creep regime. *Geophys Res Lett*. 1999;26: 251-254. doi:10.1029/1998GL900289
67. Duval P. The role of water content on the creep rate of polycrystalline ice. *IAHS*. 1977;118:29-33. PMID: https://iahs.info/uploads/dms/4722.29-33-118-Duval.pdf
68. Lliboutry L. Physical processes in temperate glaciers. *J Glaciol*. 1975; 16(74):151-158. doi:10.3189/S002214300003149X

SUPPORTING INFORMATION

Additional supporting information can be found online in the Supporting Information section at the end of this article.

How to cite this article: Thibert E, Bodin X. Changes in surface velocities over four decades on the Laurichard rock glacier (French Alps). *Permafrost and Periglac Process*. 2022; 1-13. doi:10.1002/ppp.2159